Heat Mass Transfer (2017) 53:611–623
DOI 10.1007/s00231-016-1847-9

ORIGINAL

Local distribution of wall static pressure and heat transfer on a smooth flat plate impinged by a slot air jet

Adimurthy M[1] · Vadiraj V. Katti[2]

Received: 6 January 2016 / Accepted: 31 May 2016 / Published online: 7 June 2016

Abstract Local distribution of wall static pressure and heat transfer on a smooth flat plate impinged by a normal slot air jet is experimental investigated. Present study focuses on the influence of jet-to-plate spacing (Z/D_h) (0.5–10) and Reynolds number (2500–20,000) on the fluid flow and heat transfer distribution. A single slot jet with an aspect ratio (l/b) of about 22 is chosen for the current study. Infrared Thermal Imaging technique is used to capture the temperature data on the target surface. Local heat transfer coefficients are estimated from the thermal images using 'SMART VIEW' software. Wall static pressure measurement is carried out for the specified range of Re and Z/D_h. Wall static pressure coefficients are seen to be independent of Re in the range between 5000 and 15,000 for a given Z/D_h. Nu values are higher at the stagnation point for all Z/D_h and Re investigated. For lower Z/D_h and higher Re, secondary peaks are observed in the heat transfer distributions. This may be attributed to fluid translating from laminar to turbulent flow on the target plate. Heat transfer characteristics are explained based on the simplified flow assumptions and the pressure data obtained using Differential pressure transducer and static pressure probe. Semi-empirical correlation for the Nusselt number in the stagnation region is proposed.

✉ Vadiraj V. Katti
katti.vadiraj@gmail.com

Adimurthy M
adimurthy_meda@rediffmail.com

[1] Department of Automobile Engineering, BLDEA's Dr. P G H College of Engineering and Technology, Vijayapura, Karnataka, India

[2] KLS Vishwanatharao Deshapande Rural Institute of Technology, Haliyal, Uttara Kannada, Karnataka 581329, India

List of symbols

A	Area of the smooth target surface (m^2)
A_j	Area of the slot exit (m^2)
$Avg.Nu_{2.0}$	Nusselt Number averaged up to $x/D_h = 2.0$
b	Slot width (m)
C_p	Coefficient of pressure, $C_p = \frac{2\Delta P}{\rho U_0^2}$
C_{p0}	Stagnation point ($x/D_h = 0$) Coefficient of pressure, $C_{p0} = \frac{2\Delta P_0}{\rho U_0^2}$
D_h	Hydraulic diameter of nozzle, $D_h = \frac{2bH}{b+H}$ (m)
d	Diameter of a circular jet (m)
H	Nozzle(slot) height (m)
h	Heat transfer coefficient (W/m^2K)
H_e	Equivalent height of the water column in the monometer (m), $H_e = \frac{\rho_w}{\rho_a} - 1.0$
I	Current supplied (A)
k	Thermal conductivity (W/mK)
l	Nozzle length (m)
Nu	Nusselt number based on Hydraulic diameter of the slot jet, $Nu = \frac{hD_h}{k}$
Nu_b	Nusselt number based on slot width $Nu = \frac{hb}{k}$
Nu_o	Stagnation point Nusselt number
P	Absolute wall static pressure (Pa)
ΔP	Wall static pressure at any distance from stagnation point (Pa)
ΔP_0	Wall static pressure at stagnation point (Pa)
P_o	Absolute wall static pressure at stagnation point (Pa)
q_{conv}	Net heat flux convected to the impinging jet (W/m^2)
q_{joule}	Imposed Ohmic heat flux (VI/A) (W/m^2)
q_{loss}	Total heat flux loss from impingement plate (W/m^2)
q_{nat}	Heat loss by natural convection from the back surface of impingement plate (W/m^2)

$q_{rad(b)}$	Radiation heat loss from the back surface of impingement plate (W/m^2)
$q_{rad(f)}$	Radiation heat loss from the front surface of impingement plate (W/m^2)
Re	Reynolds number based on hydraulic diameter $\left(\frac{\rho U_o D_h}{\mu}\right)$
T_{jet}	Jet air temperature (K)
T_x	Temperature of the target plate at given streamwise location (K)
U_c	Center line velocity of the free jet (m/s)
U_o	Average velocity at the nozzle exit (m/s)
U	Velocity of the jet at any given distance from the nozzle exit (m/s)
V	Voltage between the taps placed at the target plate end (V)
x	Distance on the target plate in stream wise direction (m)
Y	Nozzle to Probe distance in free jet velocity measurements (m)
Z	Jet-to-plate distance in impinging jet experiments (m)

Greek symbols

α	Thermal diffusivity of air (m^2/s)
μ	Viscosity of air (Pa s)
ν	Kinematic viscosity of air (m^2/s)
ρ_a	Density of air (kg/m^3)
ρ_w	Density of water (kg/m^3)

1 Introduction

The impingement cooling is one of the oldest and popular techniques in use, particularly for applications like the gas turbine blade cooling where heat flux is very high. Impingement cooling is highly appreciated due to its inherent character of high heat transfer rate. This kind of impinging flow devices provides short flow paths and relatively high rate of cooling for relatively small surface areas. Impinging jets are also used in the industrial processes involving high heat transfer rate, such as drying of food products, textiles, films and papers, processing of some metals and glass, cooling of gas turbine blades and outer wall of the combustion chamber, cooling of electronic equipments, etc. Due to low cost, availability and reliability, air will continue to be the working fluid. Parameters like Reynolds number (Re), jet-to-plate spacing (Z/D_h), distance from stagnation point (x/D_h) along the stream wise direction, inclination of target plate, confinement of the jet, nozzle geometry, curvature of target plate, roughness of the target plate and turbulence intensity at the nozzle exit influences the heat transfer rates of the impinging jets.

Present study concentrates on the influence of jet-to-plate spacing (Z/D_h) and Reynolds number on the Local distribution of co-efficient of wall static pressure and heat transfer due to the impinging slot air jet on smooth and flat surface. A single slot jet with an aspect ratio (l/b) of about 22 is chosen to get the fully developed flow at the nozzle exit. Reynolds number based on Hydraulic diameter (D_h) is varied from 2500 to 20,000 and jet-to-plate spacing (Z/D_h) is varied from 0.25 to 10 The local heat transfer coefficients are estimated from the thermal images obtained from infrared thermal imaging camera. Measurement for the static wall pressure is carried out for various jet-to-plate spacing's at Reynolds number varying from 2500 to 20,000. The results of the experiment are analyzed in the light of flow physics governing the given situation. The heat transfer characteristics are analyzed in the light of flow characteristics for various configurations attempted in the study.

Most of the earlier research works largely concentrated on circular jet impinging over flat and smooth surface. Review of the experimental work on heat transfer to impinging circular jets are reported by Livingood and Hrycak [1], Martin [2], Jambunathan et al. [3], Viskanta [4], Gardon and Cobonpue [5], Katti and Prabhu [6] reported the local heat transfer distribution between circular jet and flat plate. Similarly, significant amount of experimental work is reported on slot jet impinging onto a smooth flat plate by several investigators.

Gardon and Akfirat [7] studied the effect of free stream turbulence on the heat transfer between two dimensional jet and flat plate. They observed non-monotonic variation in the heat transfer in the streamwise direction especially in the regions where the mixing induced turbulence is not yet fully developed. This trend is due to the opposed effects of changes in velocity and turbulence. They identified that the stagnation point Nusselt number is maximum when jet impinges the plate near the end of its potential core region. Gardon and Akfirat [8] studied the heat transfer characteristics by a rectangular jet impinging on a smooth flat plate. They studied the characteristics for Reynolds numbers ranging from 450 to 22,000. The jet-to-plate spacing (Z/b) is varied from 0.5 to 80. They measured the temperature distribution up to x/b of 20 in the streamwise direction. They concluded that, for lower Reynolds numbers up to 2750 and jet-to-plate spacing (Z/b) less than 5, the stagnation point Nusselt number is fairly independent of nozzle width and jet-to-plate spacing. However, for higher jet-to-plate spacings (Z/b), the stagnation point Nusselt number varies with (Z/b). Nozzle width affects the Nu_o only for lower jet-to-plate spacings (Z/b) up to 10, at Reynolds number than 2750. They reported a secondary peak in the Nusselt number distribution along the streamwise direction for jet-to-plate spacing less than $9b$. Two secondary peaks are observed for jet-to-plate spacing of 0.5. The formation of secondary peak in the stagnation region is attributed to

the increasing velocities in the gap between the nozzle exit and plate.

Beitelmal et al. [9] analyzed two-dimensional impinging jets and correlated the heat transfer coefficient in the stagnation region and wall jet region with approximate solutions developed using simplified flow assumptions. They considered the jet-to-plate spacing range of $4b$ to $12b$, the Reynolds numbers ranging from 4000 to 12,000 and varied x/D_h from 1.5 to 7.5 along the streamwise direction. They observed that Nusselt number in the stagnation region is constant and explained it based on potential theory with constant thermal boundary layer thickness.

Narayanan et al. [10] studied the flow field, surface pressure and heat transfer rates of slot jet impinging on the smooth flat surface. They experimentally investigated the heat transfer distribution as the jet impinges on the flat plate within potential core region ($Z/D_h = 0.5$) and transition region ($Z/D_h = 3.0$) for jet exit Reynolds number (based on hydraulic diameter) of 23,000. They reported that, the generation of turbulence near the surface prior to impingement and the presence of vortices along the span in the stagnation region, with an increase in near wall turbulence is responsible for the enhancement in the heat transfer for the transitional jet impingement. They observed that there is a good correlation between the secondary peak in heat transfer and the peak near wall streamwise turbulence.

Zhou and Lee [11] studied the fluid flow and heat transfer characteristics by a sharp edged rectangular nozzle, for Reynolds number ranging from 2715 to 25,005 based on slot width. The jet-to-plate spacing was varied up to 30. They investigated the effect of Reynolds number, jet-to-plate spacing and turbulent intensity and found that all three variables have significant influence on the heat transfer characteristics. They proposed a correlation relating the stagnation point Nusselt number and average Nusselt number with turbulence as one of the parameter.

Tu and Wood [12] measured the shear stress and pressure measurement on the surface of target plate. They conducted the experiments for slot widths of 0.97 and 6.4 mm with Reynolds number (Re_b) ranging from 3040 to 11,000. They varied the jet-to-plate spacing (Z/D_h) up to 20. They reported that the pressure distribution follows Gaussian profile. Ashforth et al. [13] studied the velocity and turbulence at two jet-to-plate spacings (Z/D_h) of 4 and 9.2 for an orthogonally impinging slot jet generated by a convergent nozzle. It is observed that the turbulence intensity increased from the stagnation point in the stream wise direction. At around x/D_h of 2, the turbulence intensity started increasing with a large gradient and reached its peak at around x/D_h of 4. It is also observed that the turbulence intensity remains high in the region of $2 \leq x/D_h \leq 5$, which suggest that the flow undergoes a transition, which is also evident from the heat transfer measurements studied by several investigators. The turbulence intensity starts decreasing in the stream wise direction ($x/D_h > 5$) due to the excessive entrainment of quiescent surrounding air.

Zhe and Modi [14] made the velocity and turbulence measurements in the near wall along the stream wise direction from x/D_h of 1–9 to support the heat transfer data. They considered Reynolds numbers (Re_b) of 10,000, 20,000 and 30,000 and jet-to-plate spacing (Z/D_h) ranging from 2 to 8. They observed that the peak values of turbulence lies from 12 to 18 % for the downstream distances of 0.3, 1 and 5.4. They reported that, at the edge of stagnation region, shear stress reaches a minimum at x/D_h of around two. For $x/D_h > 2$, shear stress increases and reaches its maximum at x/D_h of around five. For $x/D_h > 5$, shear stress decreases monotonically.

Guo and Wood [15] measured the velocity and turbulence in the centerline of the jet. They studied the effect of jet-to-plate spacing ($Z/D_h = 2$, 4 and 5) at a Reynolds number of 83,000 based on the slot width. They reported normal stresses along the stagnation streamline for jet-to-plate spacing (Z/D_h) of 2, 4 and 5. They observed that, in the region where the mean velocity decreased, the stagnation streamwise normal stress was first amplified before being attenuated by presence of plate. With increase in the jet-to-plate spacing (Z/D_h), the normal stress also increased at all location along the stagnation streamline. The v and w component of normal stresses increased after the nozzle exit and reached its maximum well before the target plate. Further downstream, unlike u component, the v and w component normal stresses starts decreasing and reaches minimum near the target plate before its increases at the stagnation point.

It is felt from the preliminary literature studies that prior research on impinging slot jets is limited to the average heat transfer characteristics on smooth surfaces. The heat transfer rate on the impingement surface has a close relationship with flow structure at the nozzle exit. Very little work is reported on the fluid flow and heat transfer rate of impinging slot jets. Correlation of wall static pressure distribution with heat transfer from smooth surfaces is not available. Earlier researchers report no exhaustive work on the influence of fluid flow characteristics on the local distribution of the heat transfer.

Hence, the study of local heat transfer distribution and fluid flow characteristics of impinging slot air jets on flat smooth surface is proposed. In addition, it is intended to propose necessary heat transfer correlations for the various configurations studied.

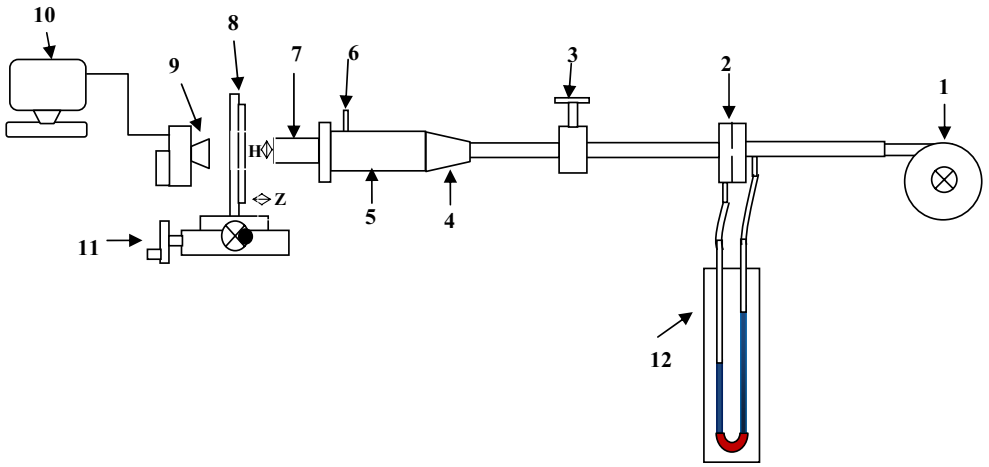

Fig. 1 Schematic layout of experiment setup for heat transfer measurement. *1* Air blower, *2* Orifice meter, *3* Flow control valve, *4* Diffuser, *5* Plenum chamber, *6* Thermo couple, *7* Slot jet, *8* Target plate, *9* Infra Red camera, *10* Computer, *11* 2-D Traverse Table, *12* U-tube monometer, H-nozzle height, Z-jet to plate distance

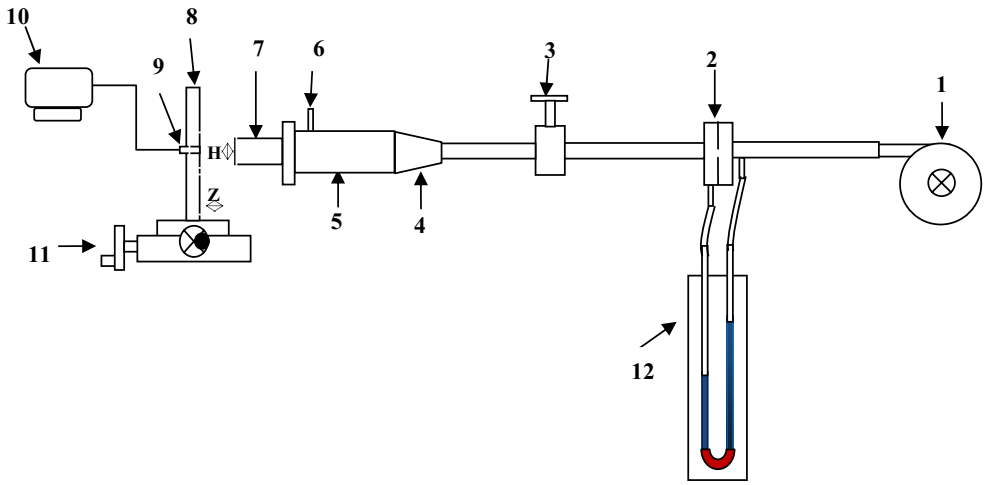

Fig. 2 Schematic layout of experiment setup for wall static pressure measurement. *1* Air blower, *2* Orifice meter, *3* Flow control valve, *4* Diffuser, *5* Plenum chamber, *6* Thermo couple, *7* Slot jet, *8* Acrylic target plate, *9* pressure tap, *10* Differential pressure transmitter, *11* 2-D Traverse Table, *12* U-tube monometer, H-nozzle height, Z-jet to plate distance

2 Experimental setup

Figures 1 and 2 respectively shows the schematic diagrams of the experimental setup for heat transfer and wall static pressure distribution studies. A blower supplies air through a calibrated orifice meter. A flow control valve of orifice meter and venturimeter controls the flow rate. To achieve the uniform flow rate at the exit of the nozzle the air is directed through a diffuser and two meshes in the plenum chamber. Velocity profile remains uniform because of the diffuser upstream of the plenum. Nozzle of dimension 90 × 4×4.5 ($l \times b \times H$) mm, made of an acrylic sheet with aspect ratio of 22, is used so that the effect of nozzle height is neglected. Jet air temperature is measured using a Chromel–Alumel Thermocouple (K-type) positioned at the inlet of the nozzle. The output of the thermocouple is

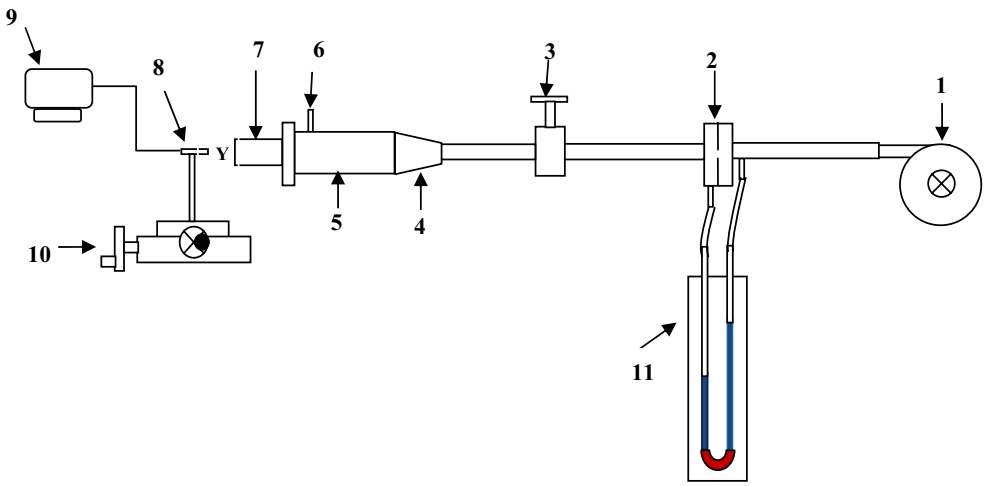

Fig. 3 Schematic layout of experiment setup for the study of free jet characteristics. *1* Air blower, *2* Orifice meter, *3* Flow control valve, *4* Diffuser, *5* Plenum chamber, *6* Thermo couple, *7* Slot jet, *8* Pitot tube, *9* Differential Pressure transmitter, *10* 2-D Traverse Table, *11* U-tube monometer, Y-jet to probe distance

measured by MECO 3.5 digit display milli voltmeter. The target plate made of 0.06 mm thick stainless steel foil is properly stretched and firmly held between the two copper bus bars is connected to regulated DC power supply. The target plate also acts as a heater. Backside of the target plate is provided with two voltage taps and is connected to a milli voltmeter to know the voltage applied to the target plate. The current supplied (*I*) can be read directly from the regulated power supply. The plate is heated to the desired temperature by controlling the voltage and current at the power supply. The plate is coated with black Asian paint matt finish at the side opposite to the impingement surface. The lateral conduction through the target plate can be neglected because of its thinness. FLUKE Ti 55 IR thermal imaging camera facing the black coated side of the target reads the temperature from the hot surface with a resolution of about 9 readings per square centimeter area of the target surface. Therefore, highly localized temperature data can be obtained from the device. Temperature data is extracted from the IR thermal images using dedicated software SMART VIEW. Thermal infrared camera reads the temperature of the plate depending on the emissivity value of the surface of the plate. Therefore, it is necessary to calibrate the emissivity of the surface. The emissivity is estimated experimentally as per found to be 0.92. The uncertainty in the temperature measurement is not more than ±0.5 °C. Power loss from the exposed surface of the target plate due to natural convection and radiation is estimated experimentally. The corrections are included in calculation of local heat transfer coefficient.

The wall pressure measurements are made on the same setup by replacing the stainless steel foil target plate with an acrylic plate as shown in Fig. 2. A static pressure tap, approximately 0.5 mm in diameter, is drilled in 10 mm thick acrylic plate for 3 mm deep from impingement surface, and then counter-bored to 3 mm diameter for the remaining depth. This pressure tap is connected to 'Furness Control' digital 'Differential Pressure Transmitter' with a range and resolution of ±1.5 kpa and ±1.0 Pa. The traversing table is moved along and across the nozzle axis to record distribution of wall static pressure.

Free jet the characteristics of a slot jet are studied using the modified set up with static pressure probe in place of the target plate on a 2-D traverse as shown in Fig. 3. The static pressure probe is connected to a Differential pressure transducer. The nozzle-probe spacing's Y/D_h is varied from 0 to10, Reynolds number is varied from 5000 to 15,000. The centerline velocity and the velocity profiles are drawn from the pressure data derived from the experiment.

3 Data reduction

The temperature distribution on the target plate is obtained by averaging ten thermal images for each configuration. Digitization of thermal images for lateral temperature distribution on impingement surface is carried out using SMART VIEW software.

The Nusselt number for the smooth surface is calculated by

$$Nu = \frac{hD_h}{k} \tag{1}$$

$$h = \frac{q_{conv}}{T_r - T_j} \quad \mathrm{W/m^2K} \tag{2}$$

Heat transfer rate between impinging jet and target plate, q_{conv}, is estimated as follows:

$$q_{conv} = q_{joule} - q_{loss} \left(\mathrm{W/m^2}\right) \tag{3}$$

$$q_{loss} = q_{rad(f)} + q_{rad(b)} + q_{nat} \left(\mathrm{W/m^2}\right) \tag{4}$$

$$q_{joule} = \frac{VI}{A} \left(\mathrm{W/m^2}\right) \tag{5}$$

$$q_{loss} = q_{rad(f)} + q_{rad(b)} + q_{nat} = \text{ Estimated experimentally} \tag{6}$$

Discharge from a calibrated venturimeter is calculated using the equation,

$$Q_{act} = C_d \left[\frac{a_1 \times a_2 \times \sqrt{(2gH_e)}}{\sqrt{(a_1^2 - a_2^2)}} \right] \mathrm{m^3/s} \tag{7}$$

a_1 = area of the venture at the inlet (m^2); a_2 = area of the venture throat (m^2)Reynolds number based on hydraulic diameter of the jet is obtained from,

$$\mathrm{Re} = \frac{\rho U_0 D_h}{\mu} \tag{8}$$

Co-efficient of wall static pressure at any point on the target plate is given by the equation,

$$C_p = \frac{2\,\Delta p}{\rho_a U_0^2} \tag{9}$$

Velocity of the jet at any point can be estimated using equation:

$$U = \sqrt{2gh}\,(\mathrm{m/s}) \tag{10}$$

Center line velocity of the jet at the nozzle exit, can be estimated using equation:

$$U_c = \sqrt{2gh}\,(\mathrm{m/s}) \tag{11}$$

Average velocity (m/s), of the jet at nozzle exit is given by,

$$U_0 = \frac{Q}{A_j} = \text{area of the slot jet}$$
$$= 0.004\,\mathrm{m} \times 0.045\,\mathrm{m} = 0.00018\,\mathrm{m^2} \tag{12}$$

A_j = area of the slot jet = 0.004 m × 0.045 m = 0.00018 m^2

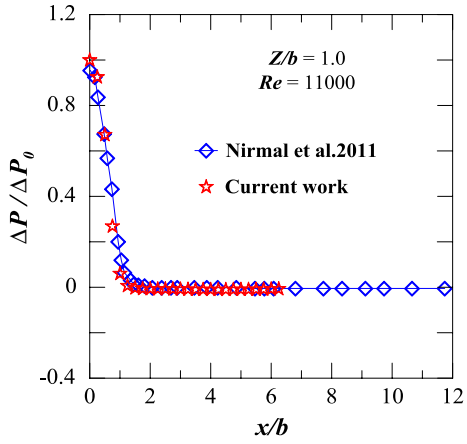

Fig. 4 Lateral distribution of Normalized pressure on the target plate for $Z/b = 1.0$, at $Re = 11{,}000$. Compared with the results of the previous researchers

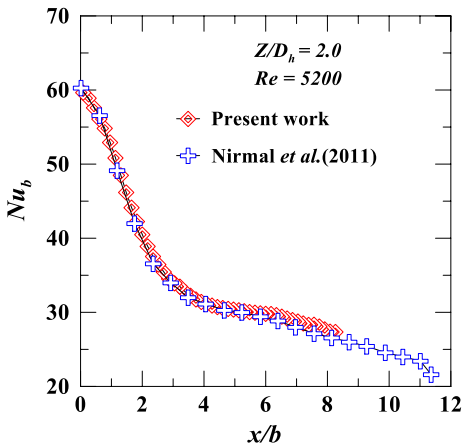

Fig. 5 Lateral distribution of Nusselt number for jet to plate distance, Z/Dh = 2.0 at Re = 5200, compared with the results of previous researchers

Uncertainties in the measurement of heat transfer coefficients are carried out using the method suggested by Moffat [17] and are around 4.2 and 2.9 % respectively at Reynolds number of 5000 and 20,000. Uncertainty in the C_p measurement is 3.4 and 2.8 % resp. at Reynolds number 5000 and 20,000.

4 Results and discussion

4.1 Comparison of the present results with the work published in literature

The experimental set up, the nozzle geometry used and the technique of temperature measurement of the present work

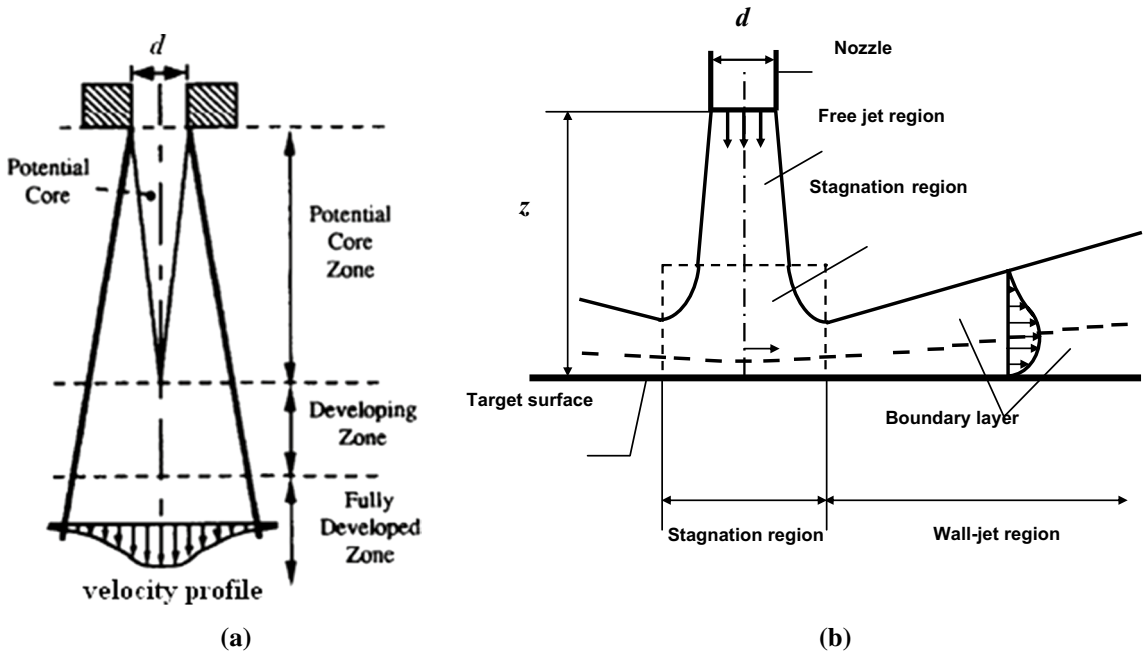

Fig. 6 Structure of submerged jet [4]. **a** Free jet, **b** Impinging jet

is exactly similar to the work of Nirmal et al. [16] hence the present work is compared with that of [16].

Figure 4 shows the distribution of normalized pressure in the stream wise direction on the target plate at Reynolds number of 11,000 for jet to plate spacing of 1.0. From the figure, it can be observed that the normalized pressure values of the current work are almost similar to that of the experimental data of Nirmal et al. [16]. The results compare well. Hence, the set up is validated for pressure measurements.

Figure 5 shows the lateral distribution of Nusselt number at slot width based Reynolds number 5200 for jet to plate spacing of 2.0. The figure shows a remarkable agreement of present results with the results of similar work from Nirmal et al. [16] and hence, the set up for heat transfer measurements is validated.

4.2 Free jet characteristics of unconfined Single slot jet: structure of free jet

The structure of free jet is as shown in the Fig. 6a. The three zones identified for the free jet are (a) Potential core zone (b) Developing zone (c) Developed zone. The jet immediately leaving the nozzle encounters surrounding stagnant air. The free shearing between moving jet and stagnant air causes the mixing due to which fluid particles of the surrounding air are carried away with the jet, which causes the sharing of the momentum of the jet and formation of the shear layer. Within the shear layer there exists a flow of jet which is still unaffected by mixing and its velocity is same as the nozzle exit velocity. This zone is *potential core* of the jet.

In the potential core zone, the centerline velocity of the jet remains constant and is equal to the nozzle exit velocity. The end of the potential core is defined as the axial distance from the nozzle exit up to the point where the jet velocity is 0.95 times the nozzle exit velocity [3]. Typical length of the potential core is found to be 6–7 times the nozzle diameter for the axi-symmetric jet and 4.7–7.7 times the slot width for two dimensional jets [4]. However, this length depends on nozzle geometry and turbulent intensity in the nozzle exit and initial velocity profile. In the developing zone, due to large shear stresses at the jet boundary, axial velocity profile decays. In the developed zone, the velocity profile is fully developed and the jet broadens linearly along with linear decay of axial velocity.

4.3 Structure of impinging jet

Figure 6b shows the flow field of an impinging jet on to an orthogonal plate. The flow structures of impinging axi-symmetric jet can be subdivided into three characteristic regions: (1) Free jet region, (2) Stagnation region, (3) Wall jet region.

The impinging jets travel from the nozzle exit as a free jet to within a distance approximately 1.2 nozzle diameters from the target plate surface [3]. Here, deceleration of flow starts and static pressure increases due to conversion of

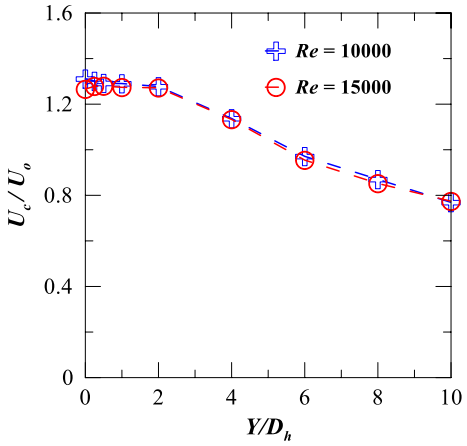

Fig. 7 Normalized centre line velocity profiles of a free jet at various Reynolds Numbers

kinetic energy of the jet. Boundary layer of constant thickness is formed at the stagnation region having a radius of ~1.1 nozzle diameters [7]. In the stagnation flow region the axial velocity component is decelerated and converts to an accelerated tangential one. The relative boundary layer thickness is found to be inversely proportional to exit Reynolds Number. Due to the exchange of momentum with stagnant surroundings and wall friction, the accelerated tangential flow transforms to a decelerated wall jet flow. It is observed that the velocity fluctuations of free jet are carried along the wall jet region also [7]. However, increase of turbulence in the wall jet region depends on turbulence in the jet prior to impingement. The heat transfer rate in the region of wall jet is found to be higher than stream wise flow over the plate. Following are some of the parameters influencing local distribution of heat transfer and fluid flow on a surface due to impinging jets. They are Reynolds number, jet-to-plate distance, radial distance from the stagnation point, confinement of jets, nozzle geometry, turbulence intensity, surface roughness, jet-to-jet distance, curvature of target surface, etc.

4.4 Centerline velocity profiles of a turbulent slot jet

An experiment is carried out to study the influence of Reynolds number on flow characteristics of free jet ejected from a slot type nozzle. The centre-line velocity profiles for the slot jet are plotted at different Reynolds numbers 10,000 and 15,000 for nozzle to probe distances (Y/D_h) ranging from zero to 10 as shown in the Fig. 7. The velocity profiles for the Reynolds numbers studied overlaps on each other, indicating that the non-dimensional velocity profiles of a turbulent slot jet are independent of Reynolds number. Maximum Velocity is observed at the jet exit for all the Reynolds numbers studied. As the distance from the nozzle exit increases the velocity decreases generally.

The velocity remains almost same as at the nozzle exit or within 5 % variation up to a nozzle to probe distance (Y/D_h) of around 2.0 and this region of the flow field can be considered as *potential core length* for the given slot jet. Potential core length is independent of the Reynolds number. The results of the Gordon and Akifirat [7] show that the potential core region for a slot jet extends up to a distance of around four nozzle widths equivalent to 2 Hydraulic diameters from the slot exit and the results obtained from current work are comparable and hence validated.

Beyond the potential core region the velocity of the jet decreases rapidly, which may be attributed to the developing jet and entrainment of atmospheric air into the jet. This trend continues up to Y/D_h of 6.0. Later the velocity of the jet decreases drastically showing a fully developed region and a diffused jet.

Figure 8 shows the variation in the normalized velocity (U/U_0) profiles of the free jet in the stream wise direction of the target plate at Reynolds number of 10,000 for different nozzle to probe distances (Y/D_h).

For the laminar jet issued from a slot jet it is observed that the maximum velocity is observed for lower nozzle to probe spacing and the velocity decreases with increase in the nozzle to probe distances (Y/D_h).

4.5 Local distributions of wall static pressure coefficients due to unconfined jet impingement

Flow study experiments are conducted to know the wall static pressure distribution over the target surface. It is found that the heat transfer coefficients are larger in the regions where the wall static pressures are high. Figure 9 shows the influence of *Re* on wall static pressure co-efficient at a given Z/D_h of 4.0 on a flat plate impinged by a normal jet. The figure reveals that for the Reynolds number ranging from 5000 to 15,000 the plots of C_p v/s x/D_h overlaps indicating that the co-efficient of pressure is independent of Reynolds number, whereas, C_p depends on the lateral position from the stagnation point on the impingement plate. The value of C_p is observed sufficiently high at the stagnation point for entire range of Reynolds numbers investigated. The decrease in the wall static pressure coefficient is very sharp up to jet to plate spacing of $x/D_h = 1.0$ for the Reynolds numbers 5000 to 15,000. The stagnation region extends up to x/D_h of around 1.5 and is a function of Z/D_h.

Figure 10 shows wall static pressure distribution on the target plate for all jet to plate spacing ($Z/D_h = 0.5$ to 10) studied at Reynolds number of 5000. The wall static pressure at the stagnation point as well as in the stream wise direction decreases with the increase in the jet to plate distance as revealed in the figure. The spread of the C_P value varies with Z/D_h and increases with it, where as peak value

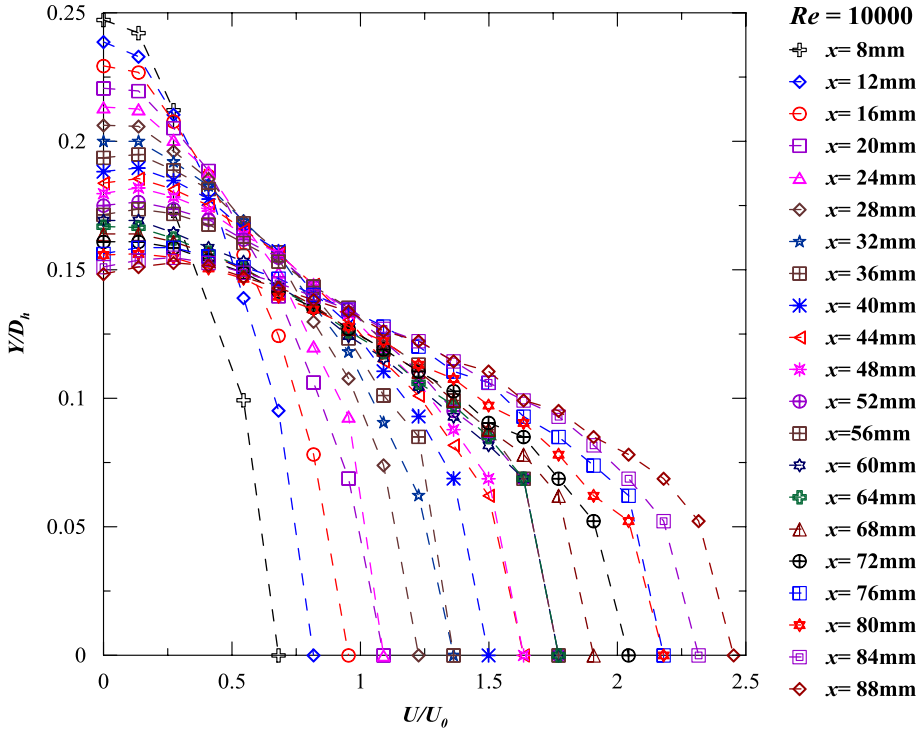

Fig. 8 Variation in the velocity profiles of an unconfined single turbulent slot jet, with nozzle to probe spacing at $Re = 10{,}000$

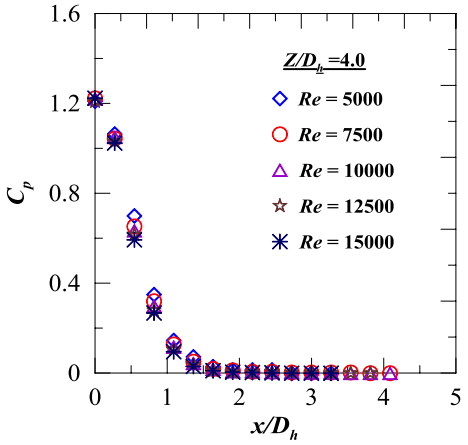

Fig. 9 Influence of Re on C_p at various lateral positions from stagnation point for $Z/D_h = 4.0$

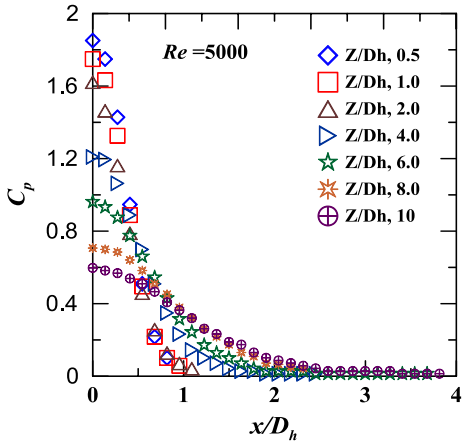

Fig. 10 Wall static pressure variation along the plate for various jet to plate spacing (Z/D_h) at $Re = 5000$

of C_p decreases with increase in Z/D_h. The value of C_P drops to zero around x/D_h of 1.0 for $Z/D_h = 0.5$ and around the 3.0 for $Z/D_h = 10$.

Figures 11 and 12 shows the variation of stagnation point wall static pressure co efficient (C_{p0}) on the plate for various Reynolds numbers ranging from 5000 to 15,000 and $Z/D_h = 0.5$ to 10. For a given Reynolds number the C_{p0} value decreases with the increase in the jet to plate distance Z/D_h. As the plate moves away from the jet, the entrainment of atmospheric air into jet begins and if the target is much beyond the potential core region, the jet starts diffusing and spread increases with reduction in the pressure on the plate. C_{p0} value is found independent of Reynolds number for the range investigated.

It is observed that the stagnation pressures are almost same for the Reynolds numbers 7500 to 15,000 showing the fully developed turbulent jet impinging on the plate. There is a little drop in pressure from Z/D_h 0.5 to 2.0, which can be attributed to the velocity of the jet, which will remain almost constant in the potential core region, which extends up to two hydraulic diameters from the nozzle exit as confirmed by the free jet analysis for the jet used in the

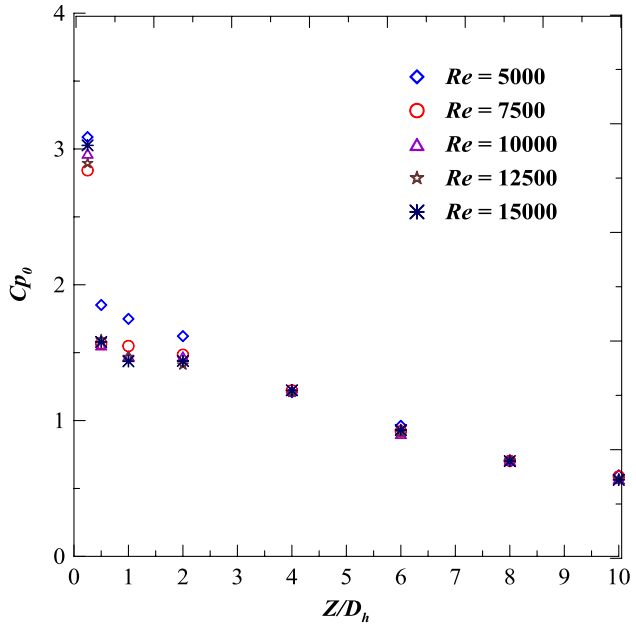

Fig. 11 Influence of *Re* on C_{p0} at various jet to plate spacing distances

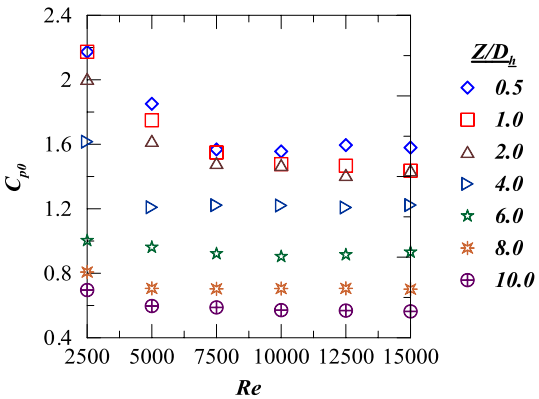

Fig. 12 Influence of Z/D_h on Cp_0 at various jet to plate spacing distances

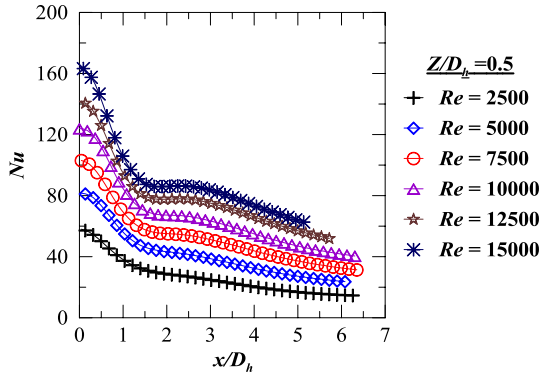

Fig. 13 Lateral variation of the Nusselt Number for $Z/D_h = 0.5$ at various Reynolds Numbers

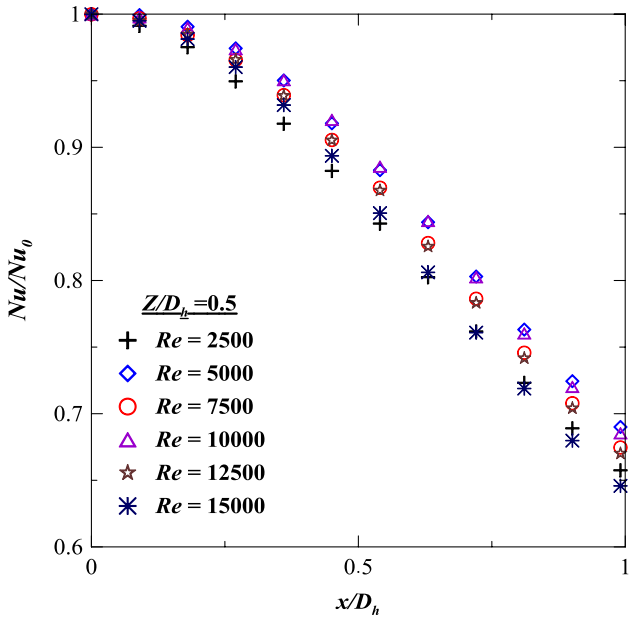

Fig. 14 Distribution of Normalized Nusselt Number in the stagnation region for $Z/D_h = 0.5$ at different *Re*

experiment. The C_{p0} value decreases for the remaining jet to plate distances studied which may be due to the fully developed jet impinging on the target plate.

4.6 Heat transfer characteristics of an unconfined single slot jet orthogonally impinging over a smooth flat surface

Experiment is conducted to study the local distribution of Heat transfer along the stream wise direction of the plate. Figure 13 reveals the influence of the *Re* on the *Nu* for a given $Z/D_h = 0.5$. Nusselt number is a function of and directly proportional to *Re* as revealed by the Fig. 10. The reason may be the increase in the mass flow rate and the velocity of the air jet with the Reynolds number. A secondary peak is observed at Reynolds number above 7500 and the peak increases with the Reynolds number, which may be attributed to the strong recirculation of the jet leading to transition from laminar to turbulent flow beyond the stagnation region on the target plate at higher Reynolds numbers.

Figures 14 and 15 show the distribution of the Normalized Nusselt Number in the stagnation region for $Z/D_h = 0.5$ and 1.0 respectively at different Reynolds numbers. In the stagnation region, which extends up to one x/D_h around the stagnation point, the normalized Nusselt number is independent of Reynolds number. The variation

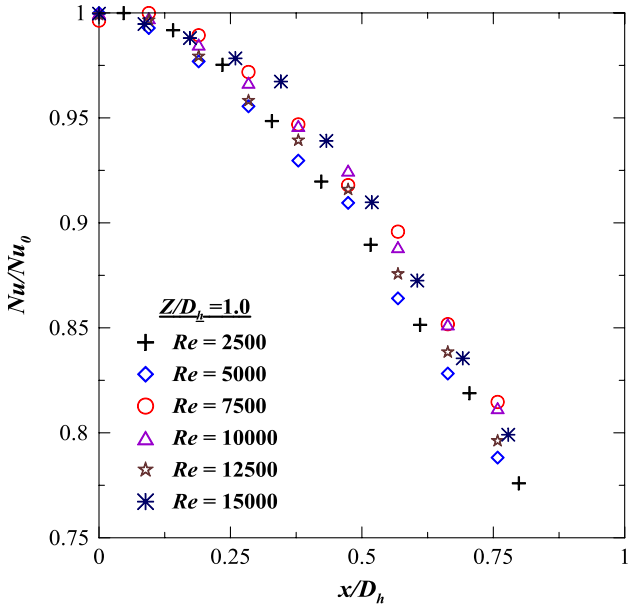

Fig. 15 Distribution of Normalized Nusselt Number (Nu/Nu_0) in the stagnation region for $Z/D_h = 1.0$ at different Re

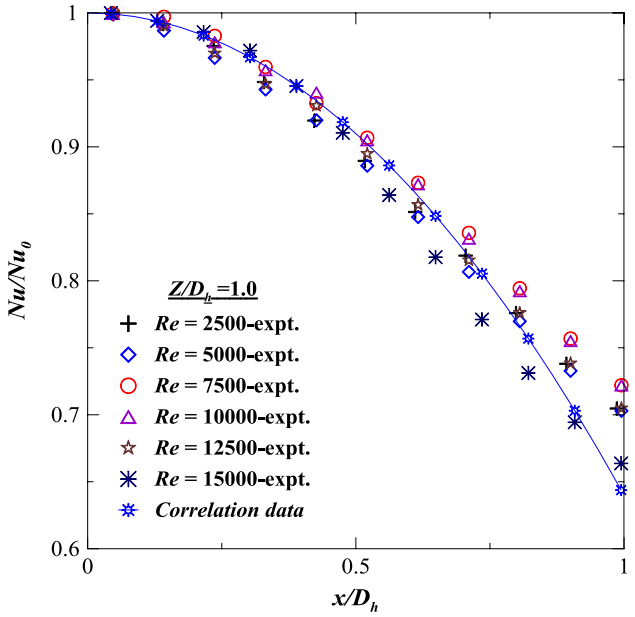

Fig. 17 Comparison of the Normalized Nusselt numbers (Nu/Nu_0) from the experiment and the correlation for $Z/D_h = 1.0$, at various Re

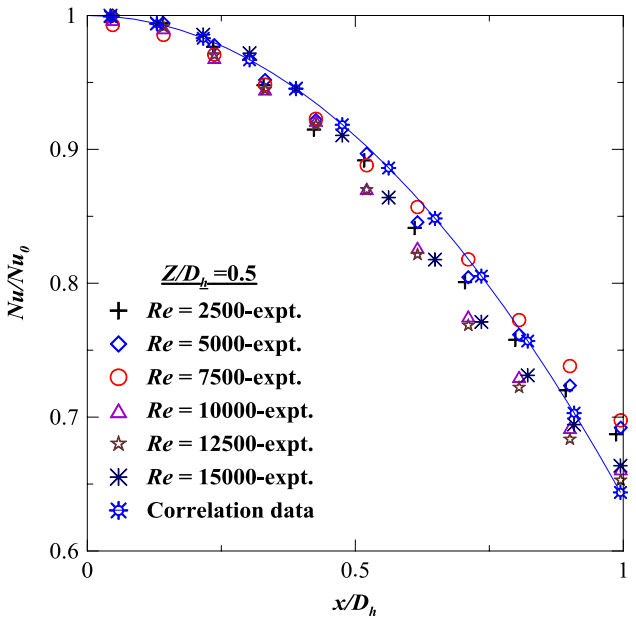

Fig. 16 Comparison of the Normalized Nusselt numbers(Nu/Nu_0) from the experiment and the correlation for $Z/D_h = 0.5$, at various Re

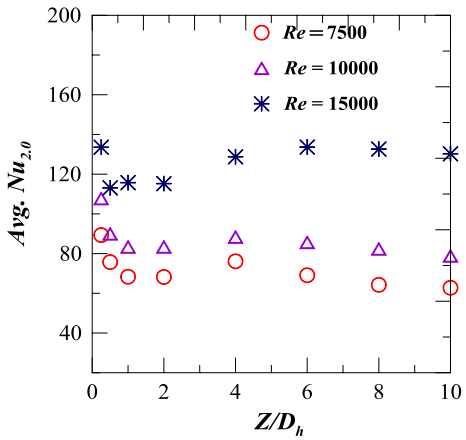

Fig. 18 Variation of Nusselt number (averaged up to $x/D_h = 2.0$) with Z/D_h and Re

in the Nu/Nu_0 value is parabolic in nature. The reason for this may be the laminar nature of the jet as it slowly and gradually picks up the speed in this region before it translates into the wall jet where it is turbulent in nature.

A correlation is developed for the Normalized Nusselt number as a function of x/D_h for jet to plate spacing (Z/D_h), below 2.0 (Stagnation region) independent of Reynolds number. The values of the Nu/Nu_0 obtained from the experiment and the data from the correlation are plotted against x/D_h at various Reynolds numbers as shown in the Figs. 16 and 17 respectively for $Z/D_h = 0.5$ and 1.0. The data compares well and fits in the acceptable range of 2 % deviation.

The correlation for estimation of normalized value of Nusselt number in the stagnation region is,

$$\frac{Nu}{Nu_0} = 1 - 0.36 \times \left(\frac{x}{D_h}\right)^2 \tag{12}$$

The correlation holds good for any jet to plate distance in the potential core region of the jet irrespective of the Reynolds number.

4.7 Variation of average Nusselt number (averaged up to $x/D_h = 2.0$) with Reynolds number and different jet to plate distances

Potential core region of the jet and stagnation region on the impinging surface are very significant for the design of any heat transfer applications may be for cooling or heating purposes. Practically x/D_h in the range of 0–2.0 is critical in industrial applications. Therefore the Nusselt number averaged up to $x/D_h = 2.0$ is considered for the analysis in the current study.

Figure 18 shows the variation of average Nusselt number with variation of jet to plate distance between 0.25 and 10 at, Reynolds numbers 7500, 10,000 and 15,000 respectively. For any given Z/D_h, the average Nusselt number increases with increase in the Reynolds number. This may be due to the increase in the mass flow rate with the Reynolds number. For any given Reynolds number, the average Nusselt number is initially high at the lower jet to plate distance and reaches its first low value around $Z/D_h = 1.0$. The Nusselt number gradually increase up to $Z/D_h = 4.0$ and reaches its second peak. With further increase in the Z/D_h, the average Nusselt number decreases gradually. When the plate moves away from the target plate, the impact of the jet weakens due to the entrainment of quiescent surrounding air and the heat transfer rate decreases. Just at the end of potential core region, the heat transfer rate will be higher at any Reynolds number around Z/D_h of 4.0 as evident from the Fig. 18.

5 Conclusions

An experimental investigation is performed to study the distribution of heat transfer coefficients between the submerged slot impinging jet and a flat smooth surface. In this study, the Reynolds number based on hydraulic diameter is varied from 2500 to 15,000 and the Z/D_h is varied from 0.25 to 10. Experiments are conducted to measure the static wall pressure distribution in the target plate from the stagnation point to x/D_h of 10.

- Heat transfer coefficients are maximum at the stagnation point($x/D_h = 0$) for a given jet-to-plate distance and Reynolds number.
- For lower jet to plate distances and higher Reynolds number, secondary peaks are observed in the heat transfer distributions. These secondary peaks may be due to fluid transiting from laminar to turbulent flow on the target plate. However, existence of secondary peaks is not prominent at lower Reynolds number.
- Wall static pressure coefficients are seen to be independent of Reynolds number in the range between 5000 and 15,000 for a given jet-to-plate distance. This may indicate self-similar behavior of the turbulent submerged jet.
- Sub atmospheric pressure region is identified for the Z/D_h of 0.25 for all the Reynolds numbers investigated. However, Sub atmospheric pressure region vanishes at higher jet-to-plate distance.
- The correlation for estimation of normalized value of Nusselt number in the stagnation region is,

$$\frac{Nu}{Nu_0} = 1 - 0.36 \times \left(\frac{x}{D_h}\right)^2$$

The correlation holds good for any jet to plate distance in the potential core region and independent of the Reynolds number.

References

1. Livingood JNB, Hrycak P(1970) Impingement heat transfer from turbulent air jets to flat plates—A literature survey, NASA Technical Memorandum (NASA TM X-2778)
2. Martin H (1977) Heat and Mass transfer between impinging gas jet and solid surface. Adv Heat Transf 13:1–60
3. Jambunathan K, Lai E, Moss MA, Button BL (1992) A review of heat transfer data for single circular jet impingement. Int J Heat Fluid Flow 13:106–115
4. Viskanta R (1993) Heat transfer to impinging isothermal gas and flame jets. Exp Thermal Fluid Sci 6:111–134
5. Gardon R, Cobonpue J (1962) Heat transfer between a flat plate and jets of air impinging on it, ASME Int. Developments in Heat Transf 454–460
6. Katti V, Prabhu SV (2008) Experimental study and theoretical analysis of local heat transfer distribution between smooth flat surface and 4 impinging air jet from a circular straight pipe nozzle. Int J Heat Mass Transf 51:4480–4495
7. Gardon R, Akfirat C (1966) Heat transfer characteristics of impinging two dimensional air jets. J Heat Transf 88:101–108
8. Gardon R, Akfirat C (1965) The Role of turbulence in determining the heat transfer characteristics of impinging jets. Int J Heat Mass Transf 8:1261–1272
9. Beitelmal AH, Shah AH, Saad MA (2006) Analysis of an impinging two dimensional jet. J Heat Transf 128:307–310
10. Narayanan V, Seyed-Yagoobi J, Page RH (2004) An experimental study of fluid mechanics and heat transfer in an impinging slot jet flow. Int J Heat Mass Transf 47:1827–1845
11. Zhou DW, Lee Sang-Joon (2007) Forced convective heat transfer with impinging rectangular jets. Int J Heat Mass Transf 50:1916–1926
12. Tu CV, Wood DH (1996) Wall pressure and shear stress measurements beneath an impinging jet. Exp Thermal Fluid Sci 13:364–373

13. Ashforth S, Jambunathan K, Whitney CF (1997) Velocity and turbulence characteristics of a semiconfined orthogonally impinging slot jet. J Exp Thermal Fluid Sci 14:60–67
14. Zhe and Modi (2001) Near wall measurements of a turbulent impinging slot jet. J Fluids Eng 123(1):112–120
15. Guo Y, Wood DH (2002) Measurements in the vicinity of a stagnation point. J Exp Thermal Fluid Sci 25:605–614
16. Nirmal Kumar M, Katti V, Prabhu SV (2011) Local heat transfer distribution on a smooth flat plate impinged by a slot jet. Int J Heat Mass Transf 54:727–738
17. Moffat RJ (1988) Describing the uncertainties in experimental results. Exp Thermal Fluid Sci 1:3–17